Korean J. Chem. Eng., 36(3), 404-410 (2019)
DOI: 10.1007/s11814-018-0197-3

pISSN: 0256-1115
eISSN: 1975-7220

Design evaluation of diesel-oxygen diffusion flame burner for start-up of high-pressure coal gasifier

Jong-Keun Park*, Changkook Ryu*,†, Sung Ho Lee, and Woohyun Jung*****

*School of Mechanical Engineering, Sungkyunkwan University, Suwon 16419, Korea
**Combustech Co. Ltd., Seoul 08506, Korea
***Plant Engineering Center, Institute for Advanced Engineering, Yongin 17180, Korea
(*Received 17 September 2018 • accepted 25 November 2018*)

Abstract−Commercial entrained-flow coal gasifiers operate at high temperatures and pressures for increased efficiency. For reduced operation costs, the start-up burner (SUB) of a gasifier requires fast heating and pressurization by intensive combustion, minimizing damage to the refractory lining and to itself. We evaluated different designs of the SUB adopting diesel-oxygen diffusion flame under the stoichiometric condition to improve the performance of the existing premixed flame burner that has been subjected to frequent failures. Using computational fluid dynamics, the combustion characteristics of the SUB with a thermal input up to 2.28 MW_{th} and pressure up to 8 bar were predicted for tests in a pilot-scale cylindrical gasifier. The results showed that the injection of diesel and oxygen through separate multiple inlets can intensify the combustion, leading to short and stable turbulent diffusion flames. Varying the design of the burner tip and inlet arrangement reduced the influence of pressure on the flame length while achieving high heat flux to the wall, which is essential for a fast and stable start-up. Further investigations are required to understand the influence of the reactor geometry on the circulation flow of high-temperature gas back to the burner tip in the actual gasifier.

Keywords: Diesel, Turbulent Diffusion Flame, Coal Gasifier, Start-up Burner

INTRODUCTION

Coal gasification is a versatile energy conversion technology for solid fuel into value-added fuel and chemical products, or directly into electricity with minimized impact on the environment. Most commercial coal gasifiers adopt entrained-flow reactors that operate at high temperatures and pressures for an efficient conversion into syngas by feeding pulverized fuel in a dry or slurry form [1,2]. The use of a high-pressure reactor is also beneficial for compact equipment sizes and the increased efficiency of the syngas utilization process.

In Korea, an integrated gasification combined cycle (IGCC) plant has recently started commercial operation at Taean (Korea Western Power Co. Ltd.). It adopted the Shell coal gasification process with an operation pressure of 42 bar and a net power output of 300 MWe. The detailed investigations for this plant have been reported in literature for the gasifier [3-5], gas quench process [6], and syngas cooler [7,8] to understand the reactions, heat transfer, and slag behaviors for operation stability and design improvement [9]. In this study, however, we focus on the start-up of the gasifier. To reduce the operational costs, the gasifier requires a fast pressurization as well as heating for start-up from the room temperature and pressure. It can be achieved by the intensive flames of a start-up burner (SUB) with a large fuel input at high pressures. The original SUB in the Taean IGCC plant adopted a premixed diesel-oxygen flame burner that used high-pressure oxygen from an air separation unit (ASU). However, this type of SUB suffered from frequent ignition failures and damages, which was one of the major issues during the commissioning and initial operation period of the plant. Such problems were also reported previously in a similar gasifier [10]. Therefore, an improvement in the burner design is required to prevent failure and damage while achieving stable operation under the same conditions of the fuel and oxidant supply.

With the benefits of high flame temperature, fast heat transfer, and increased energy efficiency, oxygen-enriched flames are used in various applications, especially in the glass-melting industry [11]. However, only a few papers have reported the specific application of diesel-oxygen flame to a SUB in a gasifier. Kuang et al. [12] reported pilot-scale tests of an SUB. The reactor was similar to the Shell gasifier, in which the SUB is located above the coal burner and inclined to the direction of the coal flame. The diesel-oxygen supply at a heat load of 120 kW/m^3 was also similar with the commercial one. They found that the reactor pressure of 9 bar halved the flame length compared to that at 1 bar, and that the flame stability was influenced by the jet deflection angle and swirl number. Yan and He [13] reported a successful application of the SUB integrating a high-energy ignitor, but no technical details were presented. Guo et al. [14] tested a hot-oxygen burner (HOB) in a bench-scale OMB gasifier. The HOB preheats O_2 using CH_4 at the central channel within the burner to facilitate the ignition of diesel for the start-up or coal-water slurry for gasification. The HOB diesel flame was more stable than the typical two-channel burner flame and could start up

†To whom correspondence should be addressed.
E-mail: cryu@me.skku.ac.kr

at a lower preheated wall temperature.

To improve the existing SUB at the Taean plant, changing the flame type to diffusion flame instead of premixed flame is proposed to prevent damage of the burner tip. However, a diffusion flame without intensive mixing may exhibit ignition delays/failures, or lengthy flames that may directly hit and damage the refractory lining. We evaluated the different designs proposed for the new SUB using computational fluid dynamic (CFD) simulations. With the mixture fraction/PDF model appropriate for the turbulent diffusion flames, four new SUB designs were analyzed for various thermal inputs and pressures up to 8 bar. From the results, the key performance data were evaluated in terms of the flame length, flow pattern, temperature, and heat flux to the wall to determine the ideal SUB design.

START-UP BURNER DESIGN AND TEST GASIFIER

1. Burner Design

Fig. 1 illustrates the four design cases of the SUB to be considered for tests in a pilot-scale gasifier. At the burner tip with a diameter of 141 mm, the inlets of the diesel and oxygen are arranged to enhance mixing differently. The diameter of each inlet is indicated in the figure. The central part of the tip in burners A and B is convex to increase the fuel-oxidant mixing by outward diesel injection, while the oxidant inlets around them are straighter toward the axial direction. Unlike burner A, the outer oxidant inlets in burner B contain a swirl. In contrast, the tip in burners C and D has a dented flat center with fuel inlets such that the oxidant jets around its edge pointing toward the center can enhance mixing. Burner C has double layers of diesel nozzles (six each) at the center, and another double layer of oxidant nozzles (eight each) at the slope and the outer flat part, respectively. Burner D has the simplest design with a single layer of diesel and oxidant nozzles, separately, in which the direction of the oxidant nozzles on the slope is toward the jets of the diesel along the axis. For burners A, B, and C having two layers for both diesel and oxidant injection, the flow rates are distributed with a ratio of 7 : 3 between the larger and smaller nozzles.

Fig. 2 shows the photographs of the water injection tests for the diesel inlets at a flow rate of 100 kg/h using N_2 as the atomizing agent. Burners A and B have jets spread to a wide angle owing to the injection on the convex center. The water spray pattern is identical

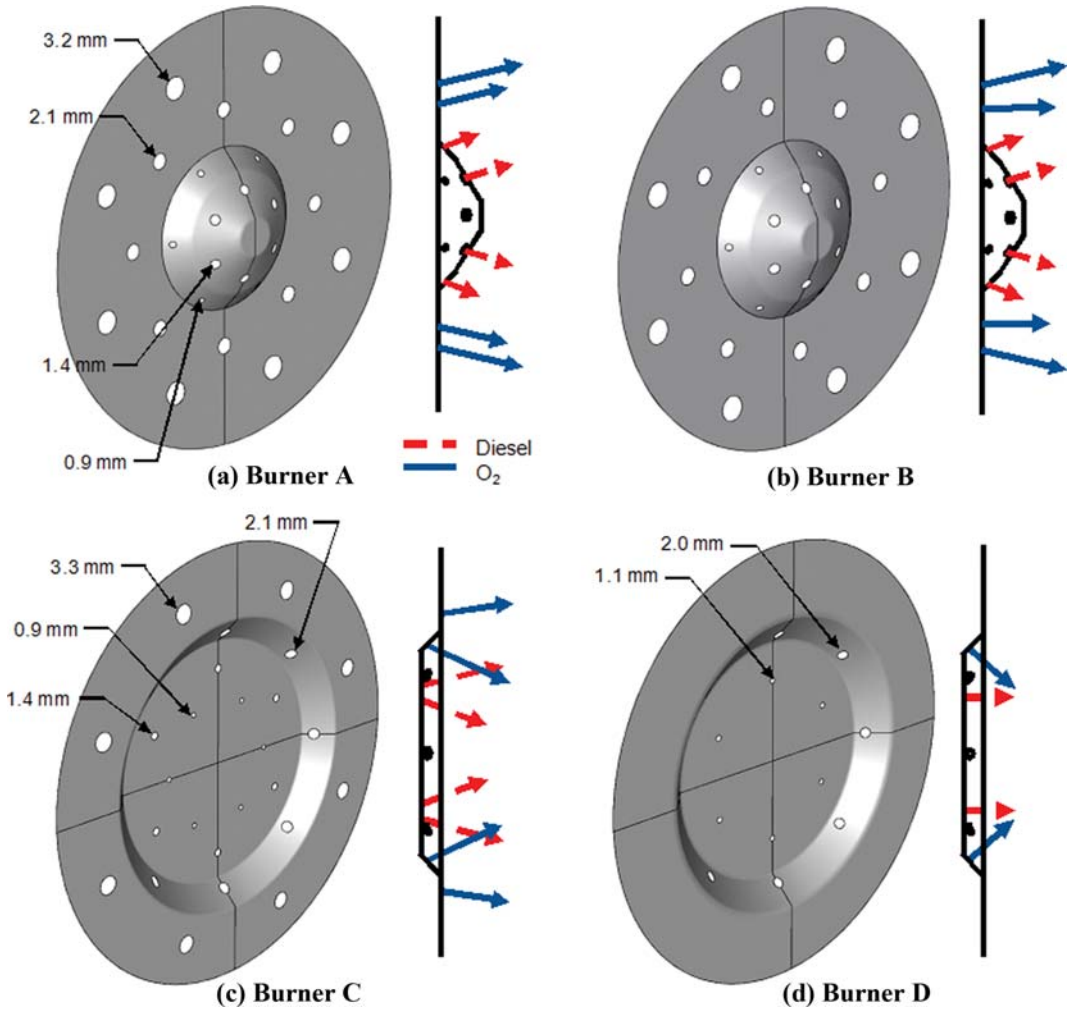

Fig. 1. Design for diesel-oxygen diffusion flame burners.

Fig. 2. Photographs of water injection tests at atmospheric pressure (water: 100 kg/h, N_2: 20 Nm^3/h).

in the two cases, because the only difference is in the swirl of the oxidant in burner B. The diesel in burner C is injected from the double layers of six nozzles each, which appear to merge into three larger jets. The water jets in burner D have the narrowest angle because of the single-layer injection.

2. Pilot-scale Gasifier

Although the SUB development is for the application in a commercial-scale gasifier, its performance is to be tested at a smaller capacity in a pilot-scale facility. Fig. 3 shows the schematic of a 3 ton/day entrained-flow coal gasifier located next to the Taean IGCC plant. It has an internal diameter of 0.5 m and a height of 6.3 m with the maximum operating pressure of 30 bar and temperature of 1,550 °C. The details of this facility and the operational data have been reported elsewhere [15]. To test the SUB, it has to be installed at the top of the gasifier, replacing the existing coal burner.

The meshes for the CFD simulation of the pilot-scale gasifier with the four SUB designs were constructed using symmetry or periodic boundary conditions appropriate for the geometry of the burner tip. The meshes for burners A (without swirl) and B (with swirl) are for half the geometry, using approximately 1.3 million hexahedral cells with symmetry and periodic conditions, separately. The meshes for burners C and D consist of approximately 1.4 million hexahedral cells with the symmetry conditions for a quarter of the geometry. The grid sensitivity was not tested, but a relatively fine mesh was used to minimize the numerical diffusion, as also shown in Fig. 3 for burner C.

NUMERICAL METHODS

CFD was applied to evaluate the performance of the burner designs and detailed combustion characteristics in the pilot-scale gasifier. This was essential to reduce the time and costs for the tests, and also to derive an appropriate start-up procedure. ANSYS Fluent (version 18.1) was used for the simulations adopting various submodels for diesel particles, combustion, turbulence, and heat transfer [16]. The diesel droplets were simulated using the discrete phase method, where the trajectories of individual droplets and their evaporation by convective and radiative heat transfer were tracked.

$$m_p c_p \frac{dT_p}{dt} = hA_p(T_\infty - T_p) - \frac{dm_p}{dt} h_{fg} + A_p \varepsilon_p \sigma(\theta_R^4 - T_p^4) \quad (1)$$

The droplet size was assumed to range from 1 μm to 50 μm with a mean diameter of 30 μm considering two-stage internal atomization process of the burner and high pressure of atomization agent (N_2). The cone angle was fixed to 10° at each inlet, which provided spray patterns reasonably close to those shown in Fig. 2. Radiation was solved by the discrete ordinate method with the weighted sum of gray gases model for gaseous absorption [17]. The turbulence

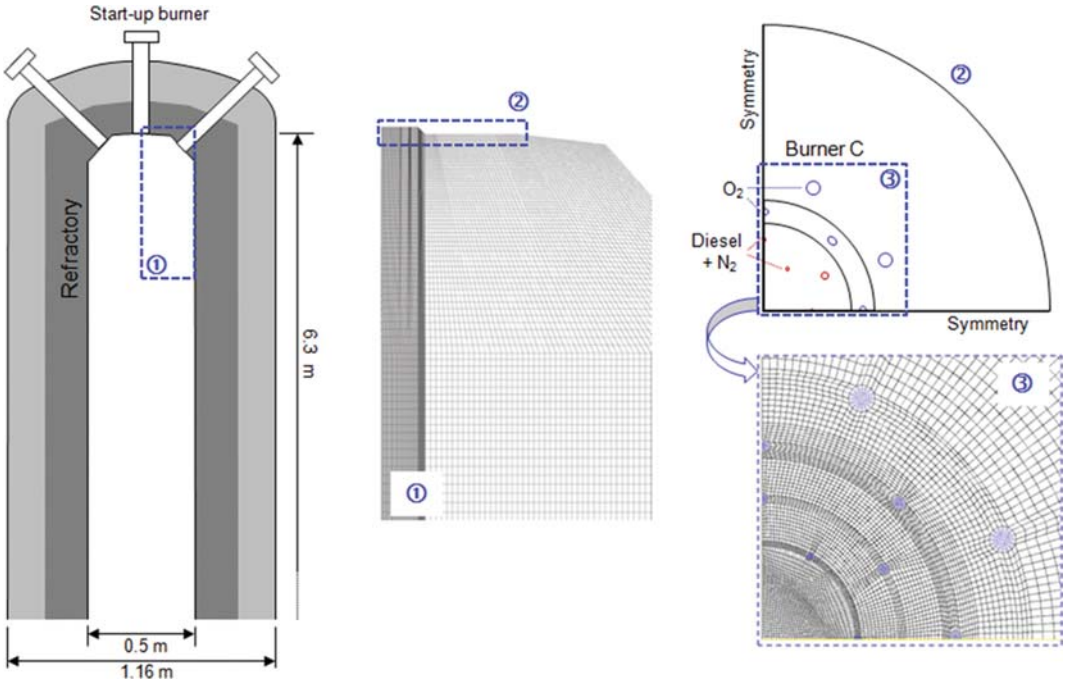

Fig. 3. Schematic of a pilot-scale (3 ton/day) coal gasifier and mesh constructed for burner C.

was solved by the realizable k-ε model, which can better predict the jet and circulating flow compared to the standard k-ε model [18].

For the chemical reaction, the mixture fraction/probability density function (PDF) model was adopted, which is ideal for the high-temperature turbulent diffusion flames of this study. The mixture fraction is defined as

$$f = \frac{Z_i - Z_{i,ox}}{Z_{i,fuel} - Z_{i,ox}}$$

where Z_i is the elemental mass fraction for element i. The subscripts fuel and ox denote the value at the fuel and oxidant stream inlets, respectively. In this model, the mixture fractions for the fuel (f_{fuel}), and secondary steam for the nitrogen as the atomizing agent (f_{sec}) are solved separately by the following conservation equations of the Favre mean (density averaged) mixture fraction and its variance [19].

$$\frac{\partial}{\partial t}(\rho\bar{f}) = \nabla\cdot(\rho\vec{v}\bar{f}) = \nabla\cdot\left(\frac{\mu_l+\mu_t}{\sigma_t}\nabla\bar{f}\right) + S_m \quad (2)$$

$$\frac{\partial}{\partial t}(\rho\overline{f'^2}) + \nabla\cdot(\rho\vec{v}\overline{f'^2}) = \nabla\cdot\left(\frac{\mu_l+\mu_t}{\sigma_t}\nabla\overline{f'^2}\right) + C_g\mu_t\cdot(\nabla\bar{f})^2 - C_d\rho\frac{\varepsilon}{k}\overline{f'^2} \quad (3)$$

The source term S_m represents the mass transfer from the liquid fuel droplets into the gas phase by evaporation. The values for constants σ_t, C_g, and C_d are 0.85, 2.86, and 2.0, respectively; μ_l and μ_t are the laminar and turbulent viscosities, respectively. The mixture fractions determine the instantaneous values of the species concentration, temperature, and physical properties under the assumption of chemical equilibrium. The turbulence-chemistry interaction was considered by the β-function of the PDF [16].

Fig. 4 shows the variations in temperature and species mole fractions determined by the chemical equilibrium calculated for the changes in f_{fuel} at the adiabatic condition. The temperature reaches a peak of 3,406 K at f_{fuel}=0.244 with thermal dissociation of species into CO, H_2, and OH (not shown) as well as CO_2 and H_2O. Higher values of f_{fuel} toward more fuel-rich conditions lead to a rapid decrease in the temperature and larger concentrations of CO, H_2, and various hydrocarbon species. A number of look-up tables similar to Fig. 4 were created for variations in the heat gain/loss and f_{sec}, which are used to determine the temperature, species, and physical properties for the two mixture fractions by interpolation.

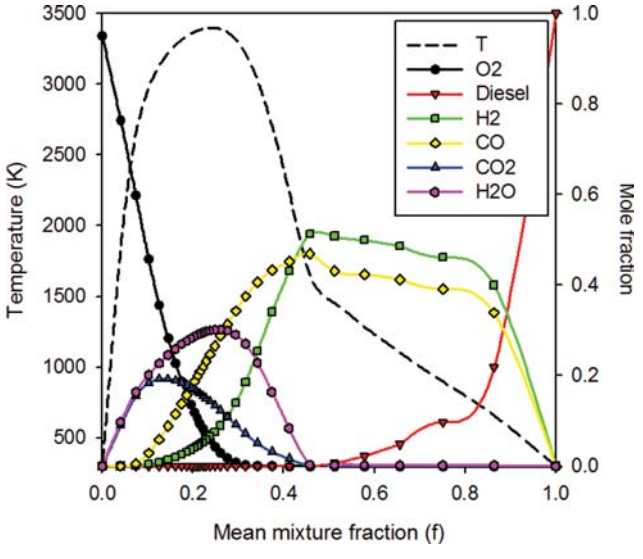

Fig. 4. Temperature and species distribution precalculated for the diesel-O flame at the adiabatic condition and f_{sec}=0.

Table 1. Operating condition of the start-up burner

Operating pressure (bar)	1	4	8
Diesel (kg/h)	40	100	180
Oxidant (O_2 95%, kg/h)	146.8	366.9	660.4
Atomizing agent (N_2, kg/h)	7.89	19.73	35.5
Inlet temperature (°C)	25	25	25
Wall temperature (K)	1000	1200	1473

Table 1 lists the operating conditions of the SUB considered in the CFD simulations. Transient simulations for a continuous pressure increase were not possible, because the pressure increase depends primarily on the downstream processes. Therefore, the operating pressures of 1, 4, and 8 bar were chosen to investigate the effect of pressure on the flame characteristics through steady-state simulations. The diesel throughput of 40, 100, and 180 kg/h (full load) was selected to compare the flame length at each respective pressure, which corresponded to a thermal input of 0.51, 1.27, and 2.28 MW_{th}, respectively. Oxygen with a purity of 95% was supplied at the stoichiometric condition with the remainder simplified as nitrogen. The wall temperature was assumed to vary from 1,000 K to 1,473 K depending on the load.

RESULTS AND DISCUSSION

Fig. 5 compares the temperature distribution at 1 bar (fuel throughput: 40 kg/h) and 8 bar (180 kg/h) conditions. At the 1 bar (40 kg/h) condition, the four burner designs lead to different temperature patterns and flame lengths. Burner D has a longer, narrower flame jet stretched to approximately 0.8 m, whereas burner C has an approximately 0.1 m shorter flame, indicating more intensive mixing between the fuel and oxygen. At the 8 bar (180 kg/h) condition, the increased fuel throughput leads to a much higher temperature (over 3,000 K) in all the burners. Depending on the burner design, the flame length can be longer (burner B) or shorter (burner D) than the respective 1 bar cases. In particular, burner D has a wider and shorter flame. Unlike the two burners, burners A and C maintain the similar flame patterns and lengths, which is favorable for a stable operation.

The temperature patterns are the result of mixing and reaction in the flame. Fig. 6 compares the O_2 mole fraction for burners C and D. Burner C has an overall similar O_2 distribution between the 1 bar and 8 bar cases. O_2 is rich at the center of the flame along the axis at 1 bar, originating from the inner oxidant inlet layer, but is depleted at 8 bar. This implies an efficient reaction at the high pressure despite the accompanying increase in the fuel throughput. In contrast, the high O_2 region created by a single oxidant inlet layer in burner D gradually becomes wider at 1 bar, and over 2% of O_2 remains up to y=0.9 m, indicating poor mixing and reaction. At 8 bar however, the O_2 distribution becomes comparable to that of burner C.

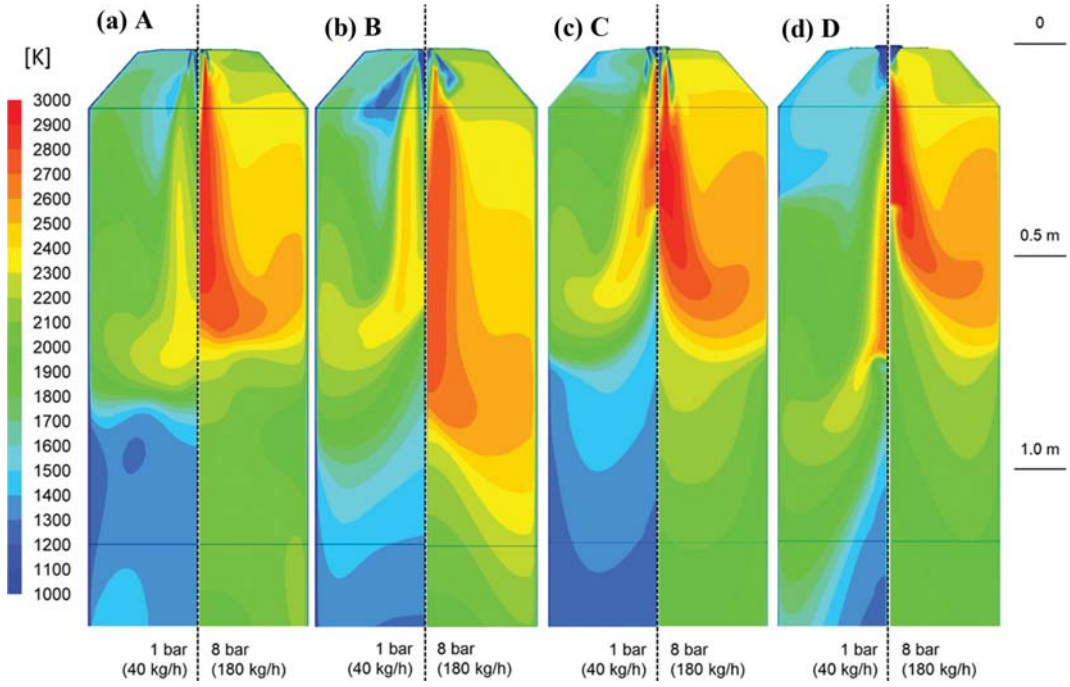

Fig. 5. Temperature contours of burners at 1 bar and 8 bar conditions with fuel throughput of 40 and 180 kg/h, respectively.

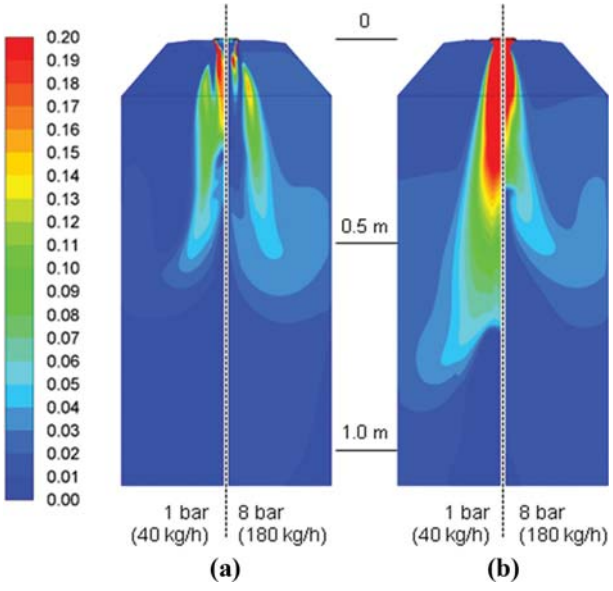

Fig. 6. Contours of O_2 mole fraction for burners (a) C and (b) D.

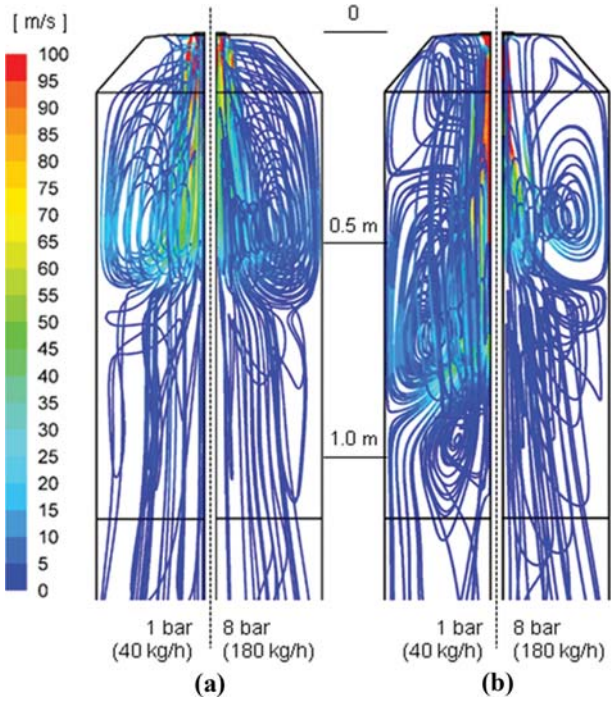

Fig. 7. Overall flow pattern of jet flames for (a) burner types C and (b) D.

Table 4 compares the flame length of the burner types, which was determined by the OH radical concentration. The criteria of the OH radical were 1% at 1 bar, 1.5% at 4 bar, and 2% at 8 bar, considering the increase in the fuel throughput. As also identified from Fig. 5, burners A and C have a relatively steady flame length, while that of burners B and D exhibit variations over the pressure range. Considering that one key requirement for the SUB design is to have a uniform flame length during start-up with a pressure increase to 8 bar, we conclude that burners A and C are appropriate. In particular, burner C has shorter flames than burner A. This can increase the heat flux to the nearby wall, which is analyzed later. Further, this short, intensive flame can deliver sufficient heat to the cold jets of coal and oxygen from the coal burner located right below after it is turned on at 8 bar. One additional issue is that burners A and B exhibit a convex tip. This shape increases the possibility of them being exposed to high temperature flows and becoming damaged; and design modifications to facilitate cooling of the burner tip are

extremely difficult. In contrast, the dented center of the burner tip in burners C and D contains spaces sufficient to insert an ignitor encircled by a nitrogen injection port for cooling and the protection of the burner tip in future development. Considering these facts, burner C appears to be the most appropriate.

Fig. 7 shows the path lines for burners C and D. In burner C for both the 1 bar and 8 bar cases, the strong jet flame along the axis loses its momentum and gradually expands towards the side wall at y=0.6 m. Part of this flow approaches the side wall and subsequently moves upward along the wall to form a recirculation zone in the upper part of the gasifier. This hot flow helps the evaporation and ignition of the fuel. In contrast, the recirculation zone is weaker in burner D with different sizes between the 1 bar and 8 bar cases. In particular, two recirculation zones are developed at 1 bar in this burner, separated approximately at y=0.34 m. The upper one close to the burner has a lower gas temperature that does not facilitate a fast ignition. In the actual gasifier, the SUB is installed above a coal burner on the side wall of the gasifier. Therefore, the aerodynamics of the recirculation flow around the burner can be extremely different than that in this pilot gasifier. Considering that the recirculation flow is induced by the strong jet flow from the burner, however, burner C is expected to have least changes over the pressure increase during the start-up. Further investigations are required regarding this.

Fig. 8 illustrates the flow and temperature pattern close to the burner tip. Burner C has two layers of oxidant nozzles, one of which is located on the outer flat part. This distributed O_2 injection reduces the intensity of flows, thus facilitating the ignition of flame close to the burner tip. In contrast, the O_2 injection is concentrated toward the focal point in burner D. Because both the diesel and oxygen are supplied at the room temperature, this concentrated cold flow delays the ignition, leading to a lifted flame, especially at 1 bar (Fig. 5). This may cause difficulties in igniting and holding the flame during the initial start-up stage at 1 bar for burner D. However, a stable operation is expected in this burner aided by the hot circulation flow at 8 bar, as shown in Fig. 8.

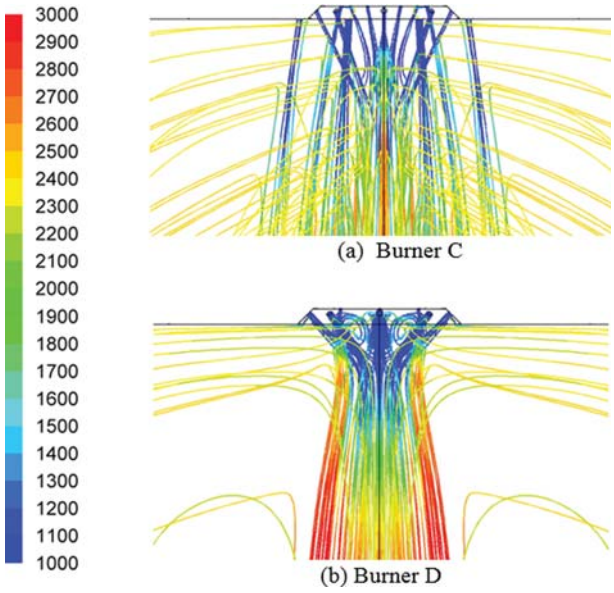

Fig. 8. Detailed flow and temperature distribution near the burner tip at 8 bar.

Fig. 9 compares the area-averaged heat fluxes on the side wall for burners C and D. The heat flux represents the amount of heat transferred to the refractory to raise its temperature that is associated with the time required for the start-up. The total and radiative heat fluxes are drawn in the figure, and the difference between them corresponds to the convective heat flux. Note that the CFD simulations assumed the steady-state at each pressure with a fixed wall temperature, ignoring the transient increase in the pressure and the corresponding accumulation of heat in the refractory lining. Therefore, the comparison of the relative trend between the cases is the primary interest rather than the absolute values. The profiles in Fig. 9 contain two regimes: (i) on the cone-shaped top wall, and (ii) on the vertical wall, separated by a dip at y=0.14 m

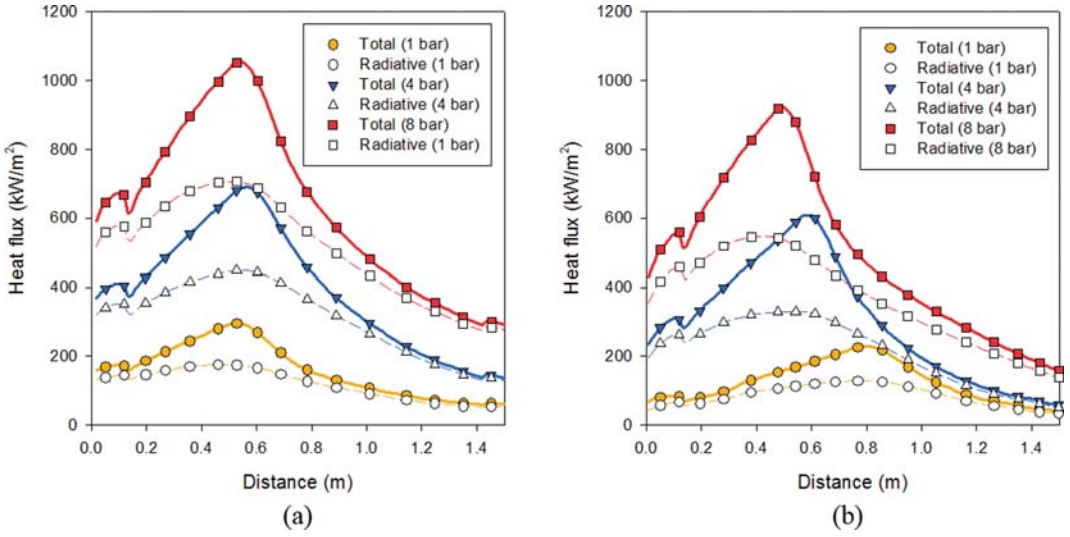

Fig. 9. Profiles of heat flux on the wall of the pilot gasifier for burners (a) C and (b) D.

Table 2. Average heat flux (kW/m^2) on the side wall of the pilot gasifier for y≤1.5 m

Pressure	1 bar	4 bar	8 bar
Burner A	142.9	311.8	581.8
Burner B	132.1	266.2	490.2
Burner C	159.8	394.5	634.5
Burner D	124.6	301.2	498.0

Table 3. Average heat flux on the tip of burner C

Pressure	1 bar	4 bar	8 bar
Radiative heat flux (kW/m^2)	135.2	327.3	588.8
Total heat flux (kW/m^2)	203.5	414.3	804.0

Table 4. Comparison of flame length (m) between burner types

Pressure	1 bar (OH: 1%)	4 bar (OH: 1.5%)	8 bar (OH: 2%)
Burner A	0.756	0.683	0.683
Burner B	0.648	0.610	0.776
Burner C	0.558	0.609	0.583
Burner D	0.733	0.606	0.548

owing to the change in the wall angle facing the flame. In both burners, the heat flux increases as the fuel throughput becomes larger at higher pressures. In each case, the maximum value of the total heat flux appears on the level where the jet flow of the flame spreads out and the hot gas flow approaches the wall. This rapidly increases the convection on top of the radiation, exhibiting relatively mild changes in the axial direction. In the total heat flux, burner C has peak points appearing at y=0.56 m, regardless of the pressures. In contrast, the point of maximum heat flux in burner D decreases by the pressure from y=0.83 m at 1 bar to y=0.51 m at 8 bar. Such trends coincide with the flame length shown in Table 4. By comparing the values between the two burners, we found that burner C has a significantly larger heat flux throughout the flame zone. This is because of the wider flame (Fig. 5).

For a quantitative analysis of the heat transfer, the average heat flux was calculated over the wall up to y=1.5 m, as compared in Table 2 for the four burner designs. Burner C has the most intensive heat flux throughout the pressures, which is favorable for a fast start-up to be ready for the introduction of coal. In contrast, burners B and D have lower values.

Finally, burner C has an important issue that requires further design improvement. Table 3 lists the heat flux on the burner tip in which burner C can have excessive heat flux by an ignition close to the tip, especially at 8 bar. The values are comparable to the peak values on the wall shown in Table 2. Therefore, the additional feature of cooling at the empty center of the burner tip would be essential for its protection, as mentioned previously.

CONCLUSIONS

Different designs of a diesel-oxygen diffusion flame burner were evaluated for the start-up of a high-pressure coal gasifier. Using CFD with a mixture fraction/PDF model, the performance of the burner design to achieve a stable and fast ignition was assessed in terms of the flame length, wall heat flux, and detailed flow pattern at the burner tip. Good mixing induced by high-speed injection through multiple inlets of oxygen and diesel led to the formation of an intensive high-temperature flame. However, changes in the burner designs led to different flame lengths over different pressures and fuel throughputs. Among these, the burner design having a dented flat center with double layers of fuel nozzles surrounded by double layers of oxidant inlets was expected to achieve a uniform flame length regardless of pressures, and a stable ignition at the burner tip during cold start at 1 bar. The intensive combustion led to excessive heat flux onto the burner tip of this design, thus requiring cooling by an internal coolant flow or by nitrogen purge at the center. Because the arrangement of the SUB at the top of the pilot gasifier was different from that for the actual gasifier at the Taean IGCC plant, further investigations are required to evaluate the effect of the reactor geometry.

ACKNOWLEDGEMENT

This work was supported by the Korea Institute of Energy Technology Evaluation and Planning (KETEP) grant funded by the Korea government Ministry of Trade, Industry, and Energy (No. 20163010050040).

REFERENCES

1. C. Higman and M. Van Der Burgt, Gulf Professional Publishing, Oxford, UK (2008).
2. D. A. Bell, B. F. Towler and M. Fan, Elsevier Inc., Oxford, UK (2011).
3. H. Lee, J. Lee, Y. Joo, M. Oh and C. Lee, *Appl. Energy*, **131**, 425 (2014).
4. C. Kim, R. Kim, Z. Wu and C. Jeon, *Korean J. Chem. Eng.*, **33**, 1767 (2016).
5. S. Park, H. Jeong and J. Hwang, *Energies*, **8**, 4216 (2015).
6. I. Ye, S. Park and C. Ryu, *Appl. Therm. Eng.*, **58**, 11 (2013).
7. S. Park, I. Ye, J. Oh, C. Ryu and J. Koo, *Appl. Therm. Eng.*, **70**(1), 388 (2014).
8. J. Oh, I. Ye, S. Park, C. Ryu and S.-K. Park, *Korean J. Chem. Eng.*, **31**, 2136 (2014).
9. M. Kim, I. Ye and C. Ryu, *Korean J. Chem. Eng.*, **35**, 1065 (2018).
10. L. Kai, Sino-Glob. *Energy*, **12**, 84 (2010).
11. Indst. Heat. Equip. Ass., DOE/GO-102008-2429, US DOE (2008).
12. J. Kuang, S. Zhang, T. Jie, F. Cao, X. Chen, H. Li and Y. Liu, Springer and Tsinghua Univ. Press, 1073 (2013).
13. C. Yan and P. He, *Guangzhou Chem. Indst.*, **40**, 142 (2012).
14. Q. Guo, Y. Gong, G. Yu, T. Wang, Y. Ma and Z. Yan, *Chem. Eng. Technol.*, **37**, 445 (2014).
15. J. Lee, S. Kang, H. Kim, D. Jeon, S. Lee, S. Chung, J. W. Lee, Y. Yun, H. Ryu and J. Baek, *Korean J. Chem. Eng.*, **33**, 2610 (2016).
16. ANSYS Inc, Canonsburg, PS (2018).
17. T. Smith, Z. Shen and J. Friedman, *J. Heat Transf.*, **104**, 602 (1982).
18. T. Shih, W. Liou, A. Shabbir, Z. Yang and J. Zhu, *Compt. Fluids*, **24**(3), 227 (1995).
19. W. Jones and J. Whitelaw, *Combust. Flame*, **48**, 1 (1982).